Korean J. Chem. Eng., 37(12), 2094-2103 (2020)
DOI: 10.1007/s11814-020-0646-7

pISSN: 0256-1115
eISSN: 1975-7220

Experiment and multiphase CFD simulation of gas-solid flow in a CFB reactor at various operating conditions: Assessing the performance of 2D and 3D simulations

Mukesh Upadhyay*,,******, Myung Won Seo*,**,†, Parlikkad Rajan Naren***, Jong-Ho Park*,**,†, Thanh Dang Binh Nguyen****, Kashif Rashid*****, and Hankwon Lim******

*Advanced Energy and Technology, Korea University of Science and Technology (UST), 217, Gajeong-ro, Yuseong-gu, Daejeon 34113, Korea
**Clean Fuel Laboratory, Korea Institute of Energy Research (KIER), 152 Gajeong-ro, Yuseong-gu, Daejeon 34129, Korea
***School of Chemical & Biotechnology, SASTRA Deemed to be University, Thanjavur, Tamil Nadu 613401, India
****School of Chemical Engineering, Hanoi University of Science and Technology, Dai Co Viet, Hanoi, Vietnam
*****Energy System Engineering, Korea University of Science and Technology (UST), 217, Gajeong-ro, Yuseong-gu, Daejeon 34113, Korea
******School of Energy and Chemical Engineering, Ulsan National Institute of Science and Technology (UNIST), 50 UNIST-gil, Eonyang-eup, Ulju-gun, Ulsan 44919, Korea
(*Received 23 January 2020 • Revised 6 July 2020 • Accepted 27 July 2020*)

Abstract−Accurate prediction of gas-solid flow hydrodynamics is key for the design, optimization, and scale-up of a circulating fluidized bed (CFB) reactor. Computational fluid dynamics (CFD) simulation with two-dimensional (2D) domain has been routinely used, considering the computational costs involved in three-dimensional (3D) simulations. This work evaluated the prediction capability of 2D and 3D gas-solid flow simulation in the lab-scale CFB riser section. The difference between 2D and 3D CFD simulation predictions was assessed and discussed in detail, considering several flow variables (superficial gas velocity, solid circulation rate, and secondary air injection). The transient Eulerian-Eulerian multiphase model was used. CFD simulation results were validated through an in-house experiment. The comparison between the experimental data and both computational domains shows that the 3D simulation can accurately predict the axial solid holdup profile. The CFD simulation comparison considering several flow conditions clearly indicated the limitation of the 2D simulation to accurately predict key hydrodynamic features, such as high solid holdup near the riser exit and riser bottom dense region. The accuracy of 2D and 3D simulations was further assessed using root-mean-square error calculation. Results indicated that the 3D simulation predicts flow behavior with higher accuracy than the 2D simulation.

Keywords: Circulating Fluidized Bed, Gas-solid Flow, Computational Fluid Dynamics, Two-fluid Model, 2D and 3D Simulation

INTRODUCTION

Gas-solid circulating fluidized bed (CFB) reactors have been widely utilized in several industrial-scale operations owing to their excellent performance, good turn-down capability, and operational flexibility [1,2]. Over the past decades, high-velocity fluidization, including turbulent and fast fluidization, has been gaining considerable interest. The fast fluidization regime is employed for the combustion of low-grade fuels, such as biomass waste and coal with high ash content [3]. Extensive research has been conducted for more than 60 years to better design and operate gas-solid CFB reactors. In particular, the focus was on understanding the underlying gas-solid flow hydrodynamics. In recent years, computational fluid dynamics (CFD) has become a cost-effective tool for predicting fluid dynamics in gas-solid fluidized bed reactors [4]. In general, the gas-solid multiphase flow can be modeled using the Eulerian-Eulerian and Eulerian-Lagrangian methods. The fundamental difference between these methods is the treatment of solid particles. In the last two decades, Eulerian-Eulerian-based two-fluid model (TFM) simulation has proven to successfully predict the gas-solid flow hydrodynamics. Although TFM simulation requires significantly lower computational resources compared to the Eulerian-Lagrangian approach, it is still extremely time consuming, particularly when industrial or large-scale three-dimensional (3D) simulation is performed [5,6]. To overcome this limitation, most of CFD reactor simulation studies found in the literature adopt two-dimensional (2D) instead of 3D simulation [7-9].

A comparative analysis between 2D and 3D simulations of a gas-solid fluidized bed reactor has been performed by several researchers. Peirano et al. [10] and Cammarata et al. [11] examined the consistency of 2D and 3D simulation results for a bubbling fluidized bed and reported significant differences between them. Reuge et al. [12] performed CFD simulations using 2D axisymmetric, 2D Cartesian, and 3D domains and concluded that 3D simulation provides accurate prediction of bubbling fluidized beds. Their comparison results also showed that the 2D Cartesian simulation

†To whom correspondence should be addressed.
E-mail: mwseo82@kier.re.kr, jongho@kier.re.kr

is better than the 2D axisymmetric simulation. However, both 2D simulations significantly overestimated the bed expansion. Asegehegn et al. [13] analyzed and compared 2D and 3D simulation results for bubbling beds with and without immersed horizontal tubes. They also concluded that 3D simulation predicts flow behavior with higher accuracy than 2D simulation. Cloete et al. [6] compared the reactor performance between 2D and 3D simulation over a wide range of flow variables in a bubbling fluidized bed reactor. They reported that 2D simulation presented qualitative predictions similar to the ones obtained by 3D simulation; however, they over-predicted the reactor performance and recommended using 2D simulation for preliminary screening studies. Xie et al. [14,15] investigated 2D and 3D simulation results for bubbling, slugging, and turbulent fluidization regimes. They concluded that the 2D simulation prediction capability declines with the increase in gas velocity and further stress on opting for 3D simulation. Recently, Bakshi et al. [16] investigated the limitations of 2D simulation for predicting gas-solid flow hydrodynamics in thin rectangular beds. They showed that 2D simulation is not able to capture bubble riser and coalescence phenomena, whereas 3D simulation successfully captured key fluidization hydrodynamics. Cardoso et al. [17] investigated the difference between 2D and 3D simulation during biomass gasification in a pilot-scale bubbling fluidized bed reactor. They observed better prediction using 3D simulation, particularly at higher superficial gas velocity. Chang et al. [18] comprehensively investigated 2D and 3D hydrodynamic models of Geldart B particles in a thin turbulent fluidized bed. They reported that both models adequately captured the bottom dense region. However, a complete 3D simulation was required to accurately capture the middle and upper region profile.

All the above mentioned studies focused on investigating bubbling and turbulent fluidized bed reactors with low superficial gas velocity. To the best of our knowledge, only one study that compared 2D and 3D simulations predicted differences for lab-scale CFB risers [19]. In all previous studies, the main fluidizing gas axially enters from the bottom inlet. However, in large-scale CFB operations, the introduction of additional reactant gas injection at a certain height above the bottom section of the riser is a common practice, known as secondary air injection [20-23]. Additionally, during long periods of operation, CFB reactors are generally operated at different superficial gas velocities and solid circulation rates [24,25]. The CFB reactor riser axial solid holdup profile shape and magnitude depend on such flow variables (superficial gas velocity, solid circulation rate, and secondary air injection) [24,26-29]. Therefore, the present work primarily aimed to identify 2D and 3D hydrodynamic simulation discrepancies considering several flow conditions. Three different sets of hydrodynamic profiles (total of seven flow conditions) were considered, representing the CFB riser operation scenario. A detailed discussion is presented to illustrate the inherent difference between 2D and 3D simulation predictions. Such a comparison study is expected to provide clear guidelines on the selection of an appropriate computational domain for gas-solid riser flow.

EXPERIMENTAL SETUP

Experiments were performed on a lab-scale CFB apparatus, as shown in Fig. 1. The CFB reactor riser has a height of 7 m and inner diameter of 0.075 m, and a bubbling fluidized bed has a height of 2 m and inner diameter of 0.2 m. The CFB riser section has an abrupt exit configuration and a secondary air injection port located 1.5 m above the gas distributor.

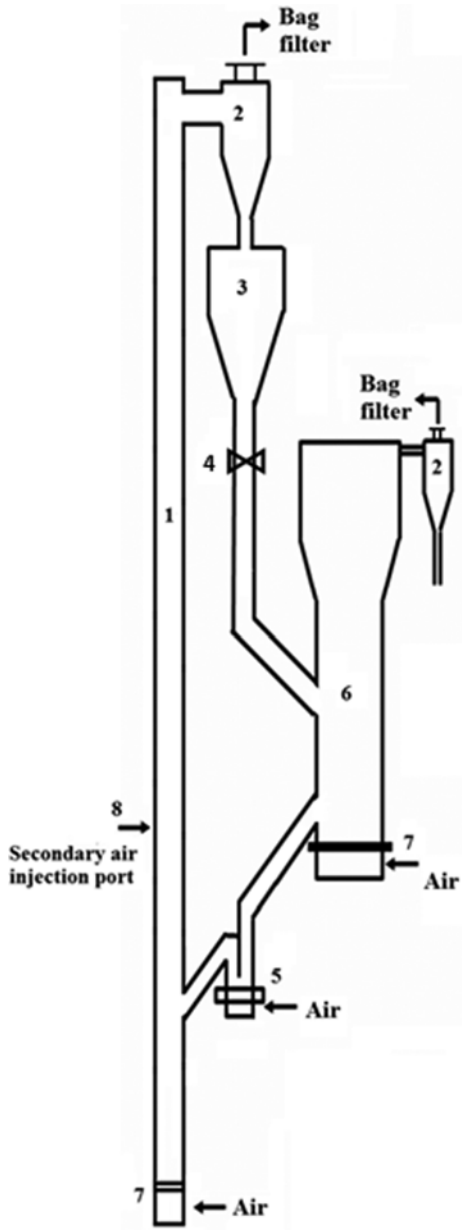

Fig. 1. Schematic diagram of the cold-rig circulating fluidized bed (CFB) reactor.

1. Riser	5. Loop seal
2. Cyclone	6. Bubbling fluidized bed
3. Hopper	7. Distributor
4. Ball valve	8. Secondary air injection port

Twelve differential pressure transducers (DPLH series, Sensys, Korea) were connected to the pressure ports along the riser column wall, and five pressure transducers were connected to the wall of a bubbling fluidized bed to measure the pressure drop. A solid inventory (I_v) of 40 kg was initially loaded into the CFB for the

experimental run. The solid particles were separated from the gas stream in the single-stage cyclone separator and returned to the bottom section of the riser through the downcomer and loop seal. The solid circulation rate was calculated by closing the ball valve below the hopper for a certain time interval and measuring the mass of solid collected therein. Experiments were performed using silica sand particles (Geldart B group) with an average diameter of 249 μm and a density of 2,353 kg/m^3. In the experiments, the gas flow rate was measured using a mass flow controller (Brooks® Model 5850E). The measured average differential pressure along the height of the riser was converted to solid holdup (ε_s) using Eq. (1) [30].

$$\frac{\Delta P}{\Delta L} = (\rho_g \varepsilon_g + \rho_s \varepsilon_s) g \cong \rho_s \varepsilon_s g \quad (1)$$

The system geometry, material properties, and flow conditions are summarized in Table 1. In the present work, axial solid holdup profiles were obtained using seven different flow conditions and classified into three sets. The first set of experiments was conducted with a constant superficial gas velocity of 3.0 m/s with different solid circulation rates. The second set was conducted at a superficial gas velocity of 4.0 and 4.5 m/s with constant solid circulation rate, whereas the third set of experiments was performed under secondary air injection condition. The secondary air injection ratio (SAR), specified as the ratio between the volumetric flow rate of gas into the secondary port and the total volumetric flow of gas, varied from 0% to 20%. The experimentally obtained axial solid holdup profiles were explained together with simulations in the Results and Discussion section.

CFD SIMULATION MODEL

Multiphase CFD simulation was based on the Eulerian-Eulerian TFM [31] approach and was performed using ANSYS® Fluent software. The TFM simulation framework constitutive equations are given in Appendix A. Detailed description of their constitutive relations can be found in other works [32-34]. To accurately predict the gas-solid flow in the CFB riser section, the partial-differential form of the granular temperature equation was used to compute the solid phase properties [35]. The popular Gidaspow drag model [32] was adopted to consider the interphase momentum exchange between the gas-solid phases. The standard k-ε turbulence model with a standard wall function was selected to simulate the gas phase turbulence. The specularity (φ) and particle-wall restitution coefficients (e_w) based on Johnson and Jackson [36] wall boundary conditions were set to 0.0001 and 0.9, respectively. The particle-particle restitution coefficient (e_{ss}) value was set to 0.9. Further, CFD simulation was performed using a transient solver with a time step of 0.0003 s with 100 iterations per time step. The phase-coupled SIMPLE scheme was employed for the pressure-velocity coupling, and additional simulation parameters used in this work are detailed in Table 2. Prior to post-processing data, the solid mass flow rate at the outlet of the CFB riser was monitored as a function of flow time to ensure that the pseudo-steady state was reached. All simulations were run for 30 s, and the results were employed by time-averaging simulation results from the last 20 s.

The 2D and 3D computational domains used for the numerical simulation are schematically shown in Fig. 2. Our previous study [37] investigated the optimum number of computational cells (not

Table 1. System geometry, material properties and flow conditions

Description	Value
System geometry:	
Riser diameter, D (m)	0.075
Riser height, H (m)	7.0
Height of the secondary air injection, h_i (m)	1.49
Material properties:	
Gas density, ρ_g (kg/m^3)	1.225
Solid particle density, ρ_s (kg/m^3)	2,353
Bulk Density (kg/m^3)	1,423
Mean particle diameter, d_p (μm)	249
Flow conditions:	
	Set-1:
	Case-1: U_g=3.0 m/s G_s=22.49±2.18 kg/m^{2}s
	Case-2: U_g=3.0 m/s G_s=44.42±0.693 kg/m^{2}s
	Case-3: U_g=3.0 m/s G_s=58.67±0.22 kg/m^{2}s
	Set-2:
	Case-4: U_g=4.0 m/s G_s=81.17±2.15 kg/m^{2}s
	Case-5: U_g=4.5 m/s G_s=81.23±1.64 kg/m^{2}s
	Set-3:
	Case-6: $U_{g(total)}$=3.0 m/s (SAR 10%) G_s=44.17±0.46 kg/m^{2}s
	Case-7: $U_{g(total)}$=3.0 m/s (SAR 20%) G_s=43.25±4.69 kg/m^{2}s

Table 2. Modeling parameters

Particle - particle and particle to wall interaction value:		
Specularity coefficient (φ)	-	0.0001
Particle-wall restitution coefficient (e_w)	-	0.9
Particle-particle restitution coefficient (e_{ss})	-	0.9
Packing limit ($\alpha_{s,max}$)	-	0.63
Run calculation and convergence settings:		
Time step (s)	-	0.0003
Convergence criteria	-	10^{-3}
Maximum number of iterations per time step	-	100
Discretization schemes settings:		
Momentum	-	Second order upwind
Volume fraction	-	QUICK
Transient formulation	-	First order implicit

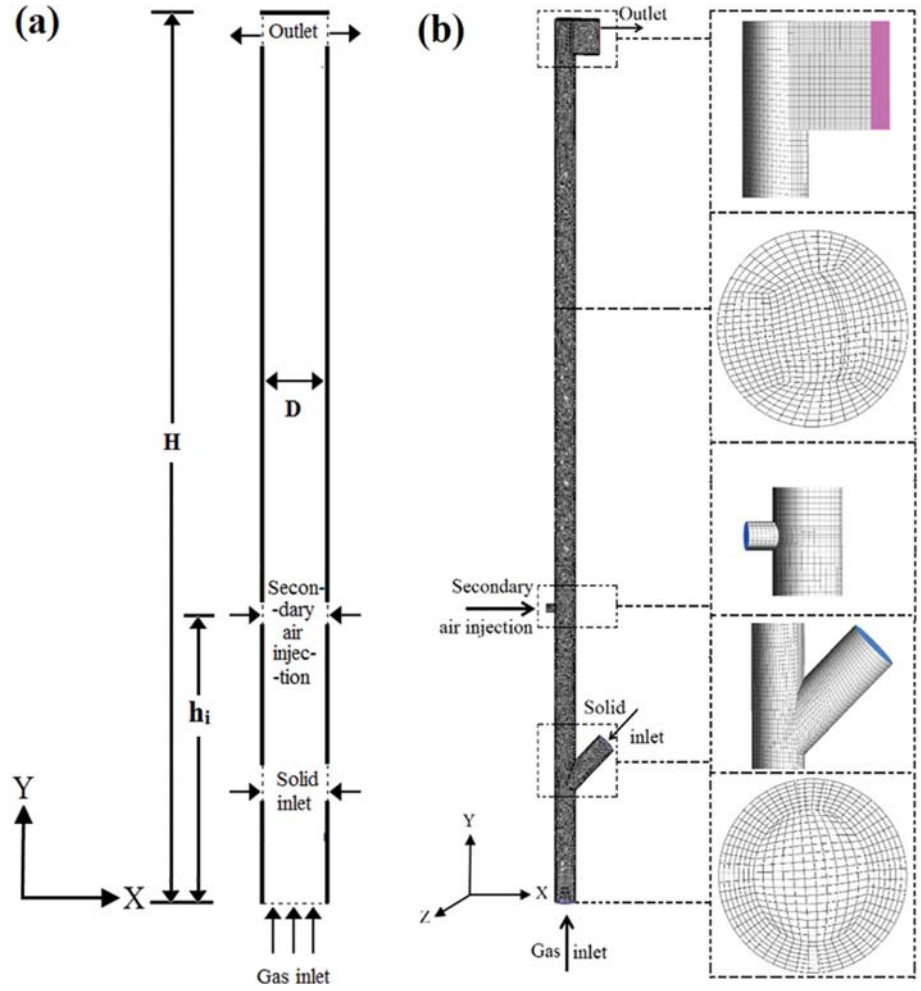

Fig. 2. Schematic diagrams of the CFB riser with secondary air injection: (a) 2D and (b) 3D computational domain.

shown here for brevity). Li et al. [38] reported that the 20-particle diameter is sufficient to ensure cell convergence criterion for the group B particle CFD simulation. From a previous work, we concluded that the cell size of 10-particle diameters ensures cell convergence criterion [38]. Therefore, in the present study, 47,250 cells for 2D and 6,21,769 cells for 3D simulations with an average cell size of 10-particle diameter were used to simulate the gas-solid flow in the riser.

RESULTS AND DISCUSSION

The gas-solid flow in the CFB riser for the flow conditions of

sets 1, 2, and 3 was simulated using 2D and 3D simulation. The axial solid holdup distribution obtained from the experiments is shown in Figs. 3(a), 4(a), and 5(a). For set-1 flow conditions, a constant superficial gas velocity (U_g=3 m/s) and increasing solid circulation rate were simulated, as shown in Figs. 3(b), (c), and (d). Both 2D and 3D simulations were able to predict the experimentally observed "nose" shape at the bottom section of the CFB riser column. The "nose" or local high solid holdup was significantly observed at a higher solid circulation rate. Fig. 3(b) shows that for a low solid circulation rate (case-1), both 2D and 3D simulation overpredicted the bottom section of the CFB riser. In contrast, for a higher solid circulation rate (case-2, case-3), the comparison be-

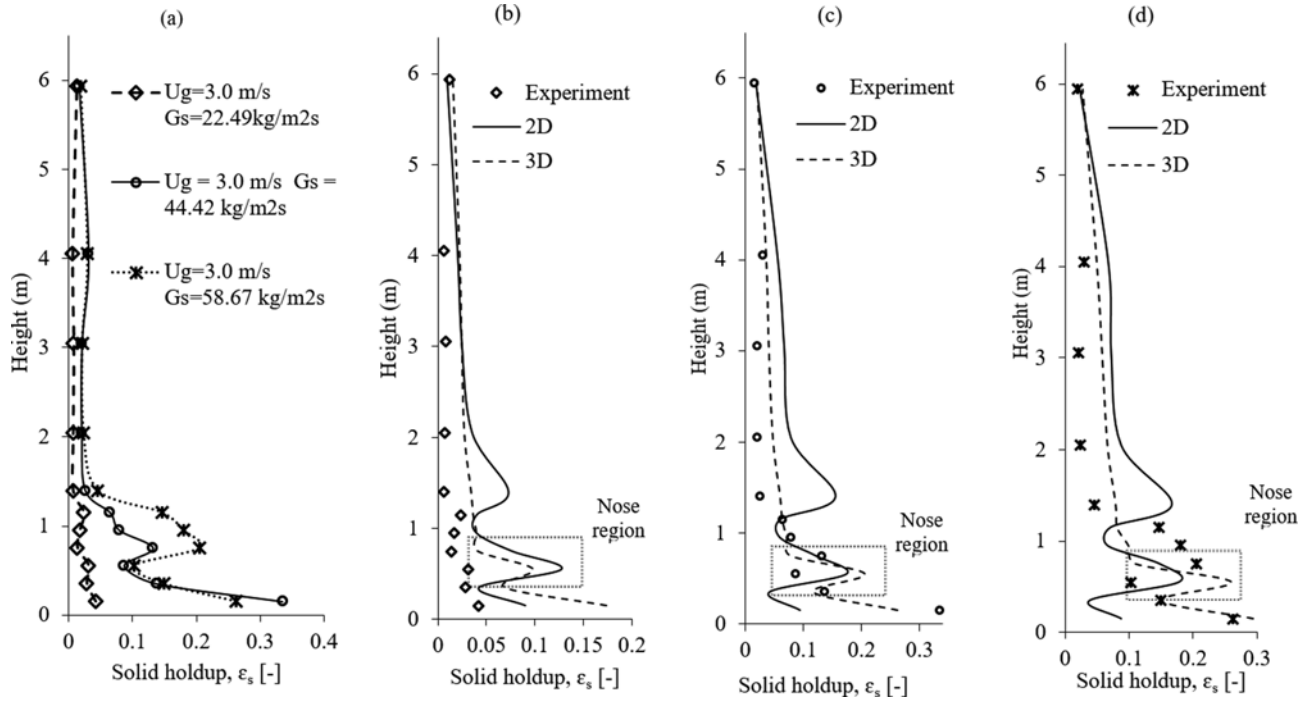

Fig. 3. Axial solid holdup profile (a) set-1 experiment data and CFD simulation comparison for (b) U_g=3.0 m/s G_s=22.49 kg/m^{2}s (c) U_g= 3.0 m/s G_s=44.42 kg/m^{2}s (d) U_g=3.0 m/s G_s=58.67 kg/m^{2}s.

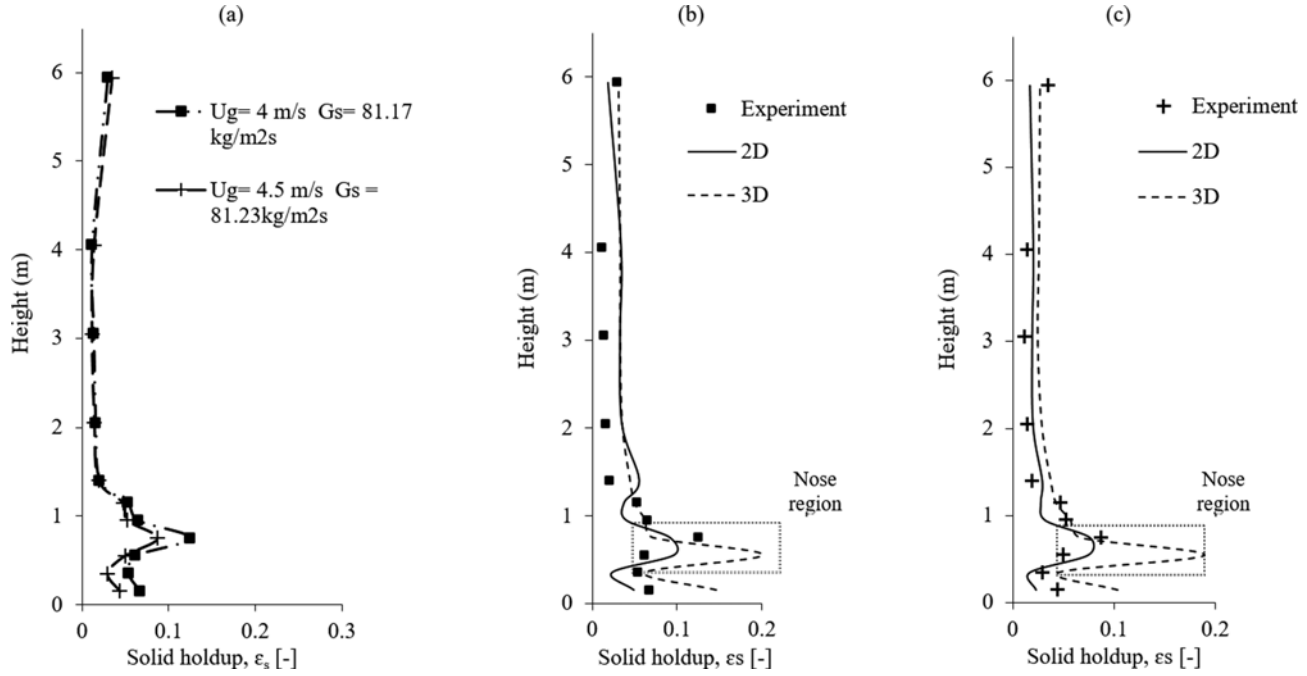

Fig. 4. Axial solid holdup profile (a) set-2 experiment data and CFD simulation comparison for (b) U_g=4 m/s G_s=81.17 kg/m^{2}s (c) U_g=4.5 m/s G_s=81.23 kg/m^{2}s.

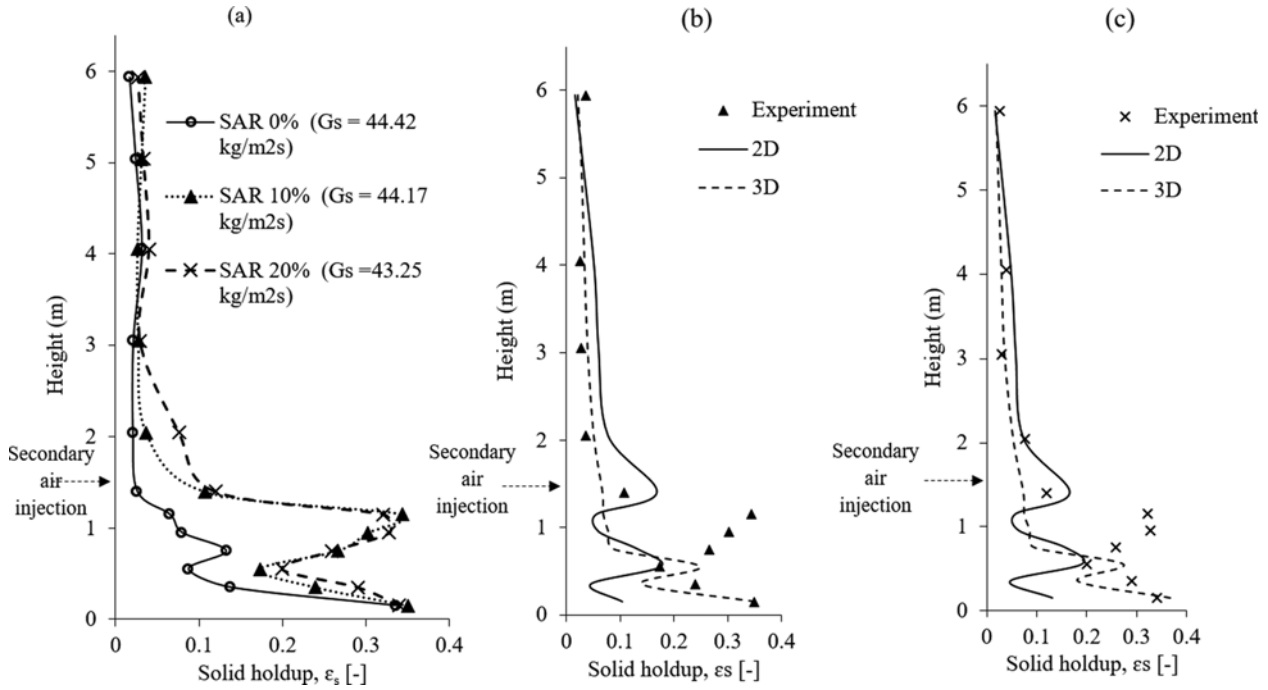

Fig. 5. Axial solid holdup profile (a) set-3 experiment data and CFD simulation comparison for (b) U_g=3.0 m/s G_s=44.17 kg/m^{2}s (SAR 10%) (c) U_g=3.0 m/s G_s=43.25 kg/m^{2}s (SAR 20%).

tween 2D and 3D clearly indicates that the 3D simulation provides a better prediction in the bottom section of the CFB riser, as shown in Figs. 3(c) and (d). For the operating conditions of set-1, the 2D simulation predicted an abnormal change in solid holdup at a height of 1.5 m, which was not supported by experimental data. However, the 3D simulation showed better consistency with the experimental data. Thus, considering these observations, 3D simulation successfully captured the experimentally observed profile.

To further verify the difference between 2D and 3D simulation, completely different flow conditions were simulated. Unlike the flow conditions of set-1, set-2 experimental data were retrieved at higher gas velocity and solid circulation rate, resulting in more solid particles in the completely developed region. At the top of the riser, owing to the abrupt exit configuration, the solid holdup was increased, as shown in Fig. 4(a). Figs. 4(b) and (c) show the 2D and 3D simulation comparison for the set-2 flow conditions. Both 2D and 3D simulation showed accurate prediction in the mid-section of the CFB riser. However, in the top section of the CFB riser, the 2D simulation failed to capture the accumulation of solid particles. Comparatively, 3D simulation could successfully capture the typical abrupt exit phenomenon. In the 3D abrupt exit configuration, some particles directly left the bed with up flowing gas, and part of the solid particles collided at the top roof, which changed the solid particle movement direction and made the particles return to the CFB riser or remain at the top cavity section. The continuous upward movement further increased the interaction and enhanced the solid concentration. However, such dynamic movement was absent in the simplified 2D geometry. A closer exam suggests that 3D simulation provides a more abrupt prediction at the bottom section of the CFB riser. In general, 2D simulation is unable to capture the typical abrupt exit profile, whereas 3D simulation shows the same flow behavior as observed in the experiment.

The 2D and 3D simulation predictions for secondary air injection flow conditions, that is, 10% and 20% SAR, are shown in Fig. 5(a). Figs. 5(b) and (c) show the comparison between 2D and 3D simulation results and experimental data. Compared to the 2D simulation, the 3D simulation provided a more reasonable agreement with the experimental data in the primary zone (bottom dense region) of the CFB riser. Moreover, the 2D simulation predicted an abrupt high solid holdup near the secondary air injection port. Above the riser height of 3 m, the difference between 2D and 3D simulation approaches was small. For the secondary air injection flow condition, the experimental measurements show that the solid holdup along the primary zone was increased due to local back mixing. It seems that it happened for both simulation approaches, completely developed at a relatively low axial distance. One possible reason for this discrepancy is the conventional Gidaspow drag model, which is unable to predict the sharp change from the dense to the dilute region in the gas-solid flow [39].

Evidently, the differences between 2D and 3D model predictions were large for the secondary air injection flow condition. Hence, the 2D and 3D simulation results were separately compared for three different SAR, that is, SAR 0% (case-2), SAR 10% (case-6), and SAR 20% (case-7), to find further ascertained differences, as shown in Fig. 6. The 3D simulation clearly predicted a reasonable tendency of increase in a solid holdup in the primary zone (bottom section) of the CFB riser compared to the 2D simulations. That is, the 3D simulation successfully captured the accumulation of particles in the primary zone. However, the 2D simulation

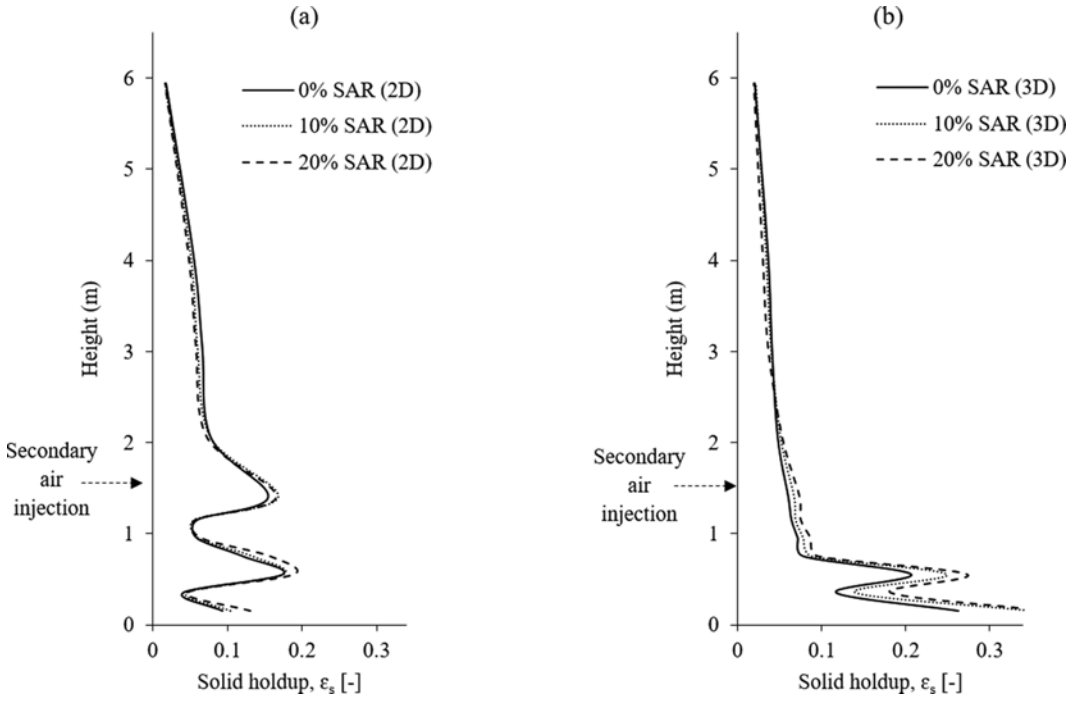

Fig. 6. CFD simulation prediction under secondary air injection ratio (SAR) flow conditions using (a) 2D and (b) 3D computational domain.

Table 3. Quantitative comparison of 2D, 3D simulation solid holdup prediction along the height of riser

Flow conditions:	Case-1		Case-2		Case-3		Case-4		Case-5		Case-6		Case-7	
Riser height (m)	2D, % deviation	3D, % deviation	2D, % deviation	3D, % deviation	2D, % deviation	3D, % deviation	2D, % deviation	3D, % deviation	2D, % deviation	3D, % deviation	2D, % deviation	3D, % deviation	2D, % deviation	3D, % deviation
0.15	114	313	72	22	67	12	27	118	47	135	70	0.14	62	8
0.35	49	141	70	15	74	1	56	16	43	51	81	42	84	37
0.55	307	214	100	137	74	154	57	15	50	282	2	44	5	37
0.75	451	194	9	41	28	47	27	43	13	24	50	67	39	63
0.95	128	129	26	10	63	45	39	3	39	8	80	74	80	74
1.15	68	52	8	2	52	45	28	5	41	11	84	80	82	77
1.4	1,011	419	502	134	264	72	171	119	54	95	58	37	38	38
2.05	424	302	285	135	273	181	122	125	41	98	115	42	3	30
3.05	218	218	219	96	238	170	144	146	68	110	123	47	99	24
4.05	234	270	76	16	128	66	194	186	46	83	95	30	21	25
5.94	26	21	9	25	22	44	37	5	51	24	54	39	37	28

predicted an abnormal change in the solid holdup near the secondary air injection port, which is inconsistent with the experimental observation. Fig. 6 shows that the solid holdup (ε_s) above the SAR port remained almost the same. Similar hydrodynamic observations were previously reported for SAR flow condition [22, 40,41]. In the present study, we clearly observed that the 2D model yielded unrealistic results. Hence, it is suggested that 3D simulation should be used for the simulation of secondary air injection flow conditions. Interestingly, if the objective of the simulation is to estimate the CFB riser holdup in the completely developed region above the secondary air injection port, the periodic computational domain can still be used with reasonable accuracy and less computational effort [42].

To quantify the difference between 2D and 3D solid holdup predictions for seven flow conditions, percentage deviations were calculated along the height of CFB riser, shown in Table 3. From data, it is clear that the percentage deviation value varies significantly at each height of riser. Therefore, overall performance of the 2D and 3D CFD simulations was assessed using the root-mean-square error (RMSE) method, described in Eq. (2).

$$\mathrm{RMSE} = \sqrt{\frac{1}{n}\sum_{i=1}^{n}\left(\varepsilon_s^{\exp eriment} - \varepsilon_s^{CFD(2D/3D)}\right)^2}, \quad (2)$$

where $\varepsilon_s^{\exp eriment}$ is the experimentally obtained solid holdup and $\varepsilon_s^{CFD(2D/3D)}$ is the solid holdup predicted from 2D and 3D CFD simulations. A smaller RMSE value indicates that the model pre-

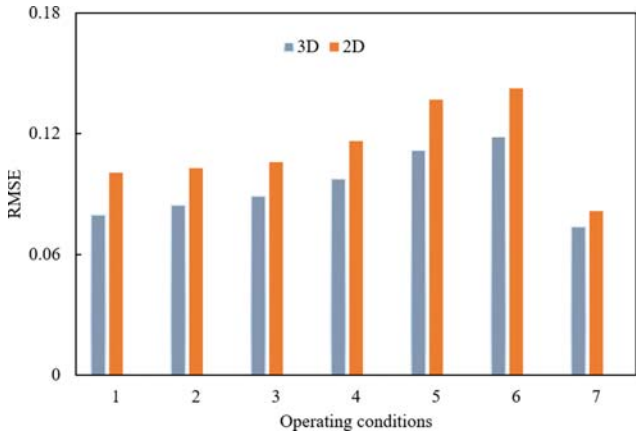

Fig. 7. Root mean square error (RMSE) of 2D and 3D CFD simulation predictions for seven different flow conditions (1: U_g= 3.0 m/s, G_s=22.49 kg/m^{2}s; 2: U_g=3.0 m/s, G_s=44.42 kg/m^{2}s; 3: U_g=3.0 m/s, G_s=58.67 kg/m^{2}s; 4: U_g=4 m/s, G_s=81.17 kg/m^{2}s; 5: U_g=4.5 m/s, G_s=81.23 kg/m^{2}s; 6: U_g=3.0 m/s, G_s=44.17 kg/m^{2}s; 7: U_g=3.0 m/s, G_s=43.25 kg/m^{2}s).

diction is closer to the experimental data. Fig. 7 displays the RMSE for 2D and 3D simulations with respect to seven different flow conditions. For the flow conditions of set 1 (case-1, case-2, case-3), the CFD simulation result with the 2D simulation showed a higher RMSE value than that of the 3D simulation, demonstrating that the 3D simulation results were closer to the experimental data. A similar performance was observed for set-2 and set-3 flow conditions, where the RMSE values for the 2D simulation were higher. However, the 2D and 3D RMSE values for set-2 (case-4, case-5) and set-3 (case-6, case-7) flow conditions were relatively higher than those for set-1. This indicates that both 2D and 3D simulations provided lower accuracy for those sets of flow conditions. Overall, the prediction accuracy was clearly lower for the 2D simulation, as evidenced by the higher RMSE values for all seven flow conditions.

CONCLUSIONS

We highlighted the limitations of 2D CFD simulation to predict gas-solid flow hydrodynamics in the riser section of a CFB reactor. An experiment was performed to obtain axial solid holdup data for several flow conditions (superficial gas velocity, solid circulation rate, and secondary air injection condition). The Eulerian-Eulerian-based classical TFM approach was used to simulate the 2D and 3D computational domains. The 2D and 3D simulation results were compared with in-house-gathered solid holdup data along the height of the CFB riser. Comparison of the first set of CFD simulations and experimental data demonstrated that the 2D simulation prediction did not capture the bottom dense region at a higher solid circulation rate. Meanwhile, comparison between measured and simulated axial solid holdup distributions for a higher gas velocity and solid circulation rate (set-2) revealed that the 2D simulation failed to predict the accumulation of solid particles near the riser exit. In addition, the 2D simulation underpredicted the bottom solid holdup compared to the 3D simulation. 2D and 3D simulations under secondary air injection conditions showed that the 3D simulation predictions were more consistent with the experimentally observed accumulation of particles in the primary zone. Major prediction differences between both computational domains were observed at the bottom and upper sections of the riser, where 2D simulation substantially underpredicted the solid holdup. Furthermore, no significant difference was observed between 2D and 3D simulation predictions in the completely developed (mid-section) region. To quantify the discrepancy between the 2D and 3D simulation predictions, we calculated the RMSE, which indicated that the 3D simulation consistently presented good predictions for all the flow conditions.

ACKNOWLEDGEMENTS

This work was conducted under the framework of the Research and Development Program of the Korea Institute of Energy Research (KIER) (B4-2433-02).

NOMENCLATURE

C_D : drag coefficient, dimensionless
d_p : mean diameter of particle [μm]
D : riser diameter [m]
e_{ss} : particle-particle restitution coefficient
e_w : particle-wall restitution coefficient
G_s : solid circulation rate [kg/m^{2}s]
g : gravitational acceleration [m/s^2]
$g_{0,ss}$: radial distribution function
H : riser Height [m]
h_i : secondary air injection height
I_v : solid inventory [kg]
k_{θ_s} : diffusion coefficient for granular energy [kg/m s]
p_i : pressure [Pa]
ΔP/ΔL : pressure drop gradient [Pa/m]
q_s : granular temperature flux at the wall
Re_i : Reynolds number
U_g : superficial gas velocity [m/s]
$\vec{U}_s$: particle slip velocity parallel to the wall
v_i : velocity [m/s]

Greek Symbols

α_i : volume fraction of phase i
$\alpha_{s,max}$: solid volume fraction at maximum packing
γ_{θ_s} : collisional dissipation of energy [kg/m^{3}s]
θ_i : granular temperature [m^2/s^2]
λ_s : solid bulk viscosity [kg/s/m]
μ_i : shear viscosity [kg/s/m]
ρ_i : density [kg/m^3]
τ_i : stress tensor for phase i [Pa]
β_{gs} : gas-solid phase interphase momentum exchange coefficient [kg/m^{3}s]
φ : specularity coefficient
ϕ_{gs} : transfer rate of energy [kg/m^{3}s]

Subscripts

col : collisional

fr : frictional
g : gas phase
kin : kinetic
s : solid phase
ss : solid-solid
w : wall

Abbreviations

2D, 3D : two-dimensional, three-dimensional
CFD : computational fluid dynamics
CFB : circulating fluidized bed
SAR : secondary air injection ratio
SIMPLE : semi-implicit method for pressure-linked equations
TFM : two-fluid model
RMSE : root mean square error

REFERENCES

1. F. Berruti, J. Chaouki, L. Godfroy, T. S. Pugsley and G. S. Patience, *Can. J. Chem. Eng.*, **73**, 569 (1995).
2. T. M. Knowlton, in *Circulating fluidized beds*, J. R. Grace, A. A. Avidan and T. M. Knowlton Eds., Blackie Academic & Professional, London, UK (1997).
3. E. U. Hartge, Y. Li and J. Werther, in *Circulating fluidized bed technology*, P. Basu, Ed., Pergamon Press, Toronto (1986).
4. J. Wang, *Chem. Eng. Sci.*, **215**, 115428 (2020).
5. T. Li, S. Benyahia, J. F. Dietiker, J. Musser and X. Sun, *Chem. Eng. Sci.*, **123**, 236 (2015).
6. S. Cloete, S. T. Johansen and S. Amini, *Powder Technol.*, **239**, 21 (2013).
7. J. H. Cloete, S. Cloete, S. Radl and S. Amini, *Powder Technol.*, **303**, 156 (2016).
8. M. T. Shah, R. P. Utikar, V. K. Pareek, M. O. Tade and G. M. Evans, *Powder Technol.*, **269**, 247 (2015).
9. S. Shah, J. Ritvanen, T. Hyppänen and S. Kallio, *Powder Technol.*, **218**, 131 (2012).
10. E. Peirano, V. Delloume and B. Leckner, *Chem. Eng. Sci.*, **56**, 4787 (2001).
11. L. Cammarata, P. Lettieri, G. D. M. Micale and D. Colman, *Int. J. Chem. Reactor Eng.*, **1**, A48 (2003).
12. N. Reuge, L. Cadoret, C. Coufort-Saudejaud, S. Pannala, M. Syamlal and B. Caussat, *Chem. Eng. Sci.*, **63**, 5540 (2008).
13. T. W. Asegehegn, M. Schreiber and H. J. Krautz, *Powder Technol.*, **219**, 9 (2012).
14. N. Xie, F. Battaglia and S. Pannala, *Powder Technol.*, **182**, 1 (2008).
15. N. Xie, F. Battaglia and S. Pannala, *Powder Technol.*, **182**, 14 (2008).
16. A. Bakshi, C. Altantzis, A. Bershanska, A. K. Stark and A. F. Ghoniem, *Powder Technol.*, **332**, 114 (2018).
17. J. Cardoso, V. Silva, D. Eusébio, P. Brito, R. M. Boloy, L. Tarelho and J. L. Silveira, *Renewable Energy*, **131**, 713 (2019).
18. J. Chang, Z. Wu, X. Wang and W. Liu, *Powder Technol.*, **351**, 159 (2019).
19. T. Li, S. Pannala and M. Shahnam, *Powder Technol.*, **254**, 115 (2014).
20. Y. J. Cho, W. Namkung, S. D. Kim and S. Park, *J. Chem. Eng. Jpn.*, **27**, 158 (1994).
21. L. E. Ersoy, M. R. Golriz, M. Koksal and F. Hamdullahpur, *Powder Technol.*, **145**, 25 (2004).
22. M. Koksal and F. Hamdullahpur, *Chem. Eng. Res. Des.*, **82**, 979 (2004).
23. W. Namkung and S. D. Kim, *Powder Technol.*, **113**, 23 (2000).
24. K. Smolders and J. Baeyens, *Powder Technol.*, **119**, 269 (2001).
25. J. Li, Y. Tung and M. Kwauk, in *Circulating fluidized bed technology II*, P. Basu and J. F. Large Eds., Pergamon Press, New York, U.S.A. (1988).
26. A. T. Harris, J. F. Davidson and R. B. Thorpe, *AIChE J.*, **49**, 52 (2003).
27. J. D. Wilde, G. B. Marin and G. J. Heynderickx, *Chem. Eng. Sci.*, **58**, 877 (2003).
28. S. K. Gupta and F. Berruti, *Powder Technol.*, **108**, 21 (2000).
29. H. Takeuchi, T. Hirama, T. Chiba, J. Biswas and L. S. Leung, *Powder Technol.*, **47**, 195 (1986).
30. U. Arena, A. Cammarota and L. Pistone, in *Circulating fluidized bed technology*, P. Basu, Ed., Pergamon Press, Toronto (1986).
31. T. B. Anderson and R. Jackson, *Ind. Eng. Chem. Fundam.*, **6**, 527 (1967).
32. M. Upadhyay and J. H. Park, *Powder Technol.*, **272**, 260 (2015).
33. S. Benyahia, M. Syamlal and T. J. O'Brien, *Powder Technol.*, **156**, 62 (2005).
34. B. Jin, X. Wang, W. Zhong, H. Tao, B. Ren and R. Xiao, *Energy Fuels*, **24**, 3159 (2010).
35. Y. Zhang, F. Lei, S. Wang, X. Xu and Y. Xiao, *Powder Technol.*, **280**, 227 (2015).
36. P. C. Johnson and R. Jackson, *J. Fluid Mech.*, **176**, 67 (1987).
37. M. Upadhyay, M. W. Seo, N. S. Nho and J. H. Park, *Comp. Aided Chem. Eng.*, **37**, 695 (2015).
38. A. T. Andrews IV, P. N. Loezos and S. Sundaresan, *Ind. Eng. Chem. Res.*, **44**, 6022 (2005).
39. M. T. Shah, R. P. Utikar, M. O. Tade and V. K. Pareek, *Chem. Eng. J.*, **168**, 812 (2011).
40. Y. Kang, P. S. Song, J. S. Yun, Y. Y. Jeong and S. D. Kim, *Chem. Eng. Commun.*, **177**, 31 (2000).
41. M. Koksal and F. Hamdullahpur, *Chem. Eng. Commun.*, **192**, 1151 (2005).
42. P. R. Naren and V. V. Ranade, *Particuology*, **9**, 121 (2011).

APPENDIX A

A.1. Continuity and Momentum Conservation Equations

- Gas-phase continuity equation:

$$\frac{\partial}{\partial t}(\alpha_g\rho_g)+\nabla\cdot(\alpha_g\rho_g\vec{v}_g)=0 \tag{A.1}$$

- Solid-phase continuity equation:

$$\frac{\partial}{\partial t}(\alpha_s\rho_s)+\nabla\cdot(\alpha_s\rho_s\vec{v}_s)=0 \tag{A.2}$$

- Gas-phase momentum conservation equation:

$$\frac{\partial}{\partial t}(\alpha_g\rho_g\vec{v}_g)+\nabla\cdot(\alpha_g\rho_g\vec{v}_g\vec{v}_g) = -\alpha_g\nabla p+\nabla\cdot\bar{\bar{\tau}}_g+\alpha_g\rho_g g+\beta_{sg}(\vec{v}_s-\vec{v}_g) \tag{A.3}$$

- Solid-phase momentum conservation equation:

$$\frac{\partial}{\partial t}(\alpha_s\rho_s\vec{v}_s)+\nabla\cdot(\alpha_s\rho_s\vec{v}_s\vec{v}_s) = -\alpha_s\nabla p-\nabla p_s+\nabla\cdot\bar{\bar{\tau}}_s+\alpha_s\rho_s g+\beta_{sg}(\vec{v}_g-\vec{v}_s) \tag{A.4}$$

- Solid and gas-phases stress tensors:

$$\bar{\bar{\tau}}_s=\alpha_s\mu_s(\nabla\vec{v}_s+\nabla\vec{v}_s^{\,T})+\alpha_s\left(\lambda_s-\frac{2}{3}\mu_s\right)\nabla\cdot\vec{v}_s\bar{\bar{I}}$$

$$\bar{\bar{\tau}}_g=\alpha_g\mu_g(\nabla\vec{v}_g+\nabla\vec{v}_s^{\,T})-\frac{2}{3}\nabla\cdot\vec{v}_g\bar{\bar{I}}$$

A.2. Interphase Momentum-exchange Coefficient

- Gidaspow drag model

$$\beta_{sg}^{Ergun}=150\frac{\alpha_s^2\mu_g}{\alpha_g d_s^2}+1.75\frac{\alpha_s\rho_g|\vec{v}_s-\vec{v}_g|}{d_s},\ \text{for } \alpha_g\le 0.8$$

$$\beta_{sg}^{Wen\text{-}Yu}=\frac{3}{4}C_D\frac{\alpha_s\alpha_g\rho_g|\vec{v}_s-\vec{v}_g|}{d_s}\alpha_g^{-2.65},\ \text{for } \alpha_g>0.8 \tag{A.5}$$

where

$$C_D=\frac{24}{\alpha_g Re_s}[1+0.15(\alpha_g Re_s)^{0.687}]$$

$$Re_s=\frac{\rho_g d_s|\vec{v}_s-\vec{v}_g|}{\mu_g}$$

A.3. Kinetic Theory of Granular Flow (KTGF)

- Granular-temperature equation:

$$\frac{3}{2}\left[\frac{\partial}{\partial t}(\rho_s\alpha_s\theta_s)+\nabla\cdot(\rho_s\alpha_s\vec{v}_s\theta_s)\right] = (-p_s\bar{\bar{I}}+\bar{\bar{\tau}}_s):\nabla\vec{v}_s+\nabla\cdot(k_{\theta_s}\nabla\theta_s)-\gamma_{\theta_s}+\phi_{sg} \tag{A.6}$$

$(-p_s\bar{\bar{I}}+\bar{\bar{\tau}}_s):\nabla\vec{v}_s$=Generation of energy by the solid stress tensor

Collisional energy dissipation

$$\gamma_{\theta_s}=\frac{12(1-e_{ss}^2)g_{0,ss}}{d_p\sqrt{\pi}}\rho_s\varepsilon_s\theta_s^{3/2}$$

Diffusion coefficient for granular energy:

$$k_{\theta_s}=\frac{150d_s\rho_s\sqrt{\theta_s\pi}}{384(1+e_{ss})g_{0,ss}}\left[1+\frac{6}{5}\alpha_s g_{0,ss}(1+e_{ss})\right] +2\rho_s\alpha_s^2 d_s(1+e_{ss})g_{0,ss}\sqrt{\frac{\theta_s}{\pi}} \tag{A.7}$$

where

$\phi_{sg}=-3K_{gs}\theta_s$ energy exchange between fluid and solid phases

- Solid pressure:

$$P_s=\alpha_s\rho_s\theta_s+2\rho_s(1+e_{ss})\alpha_s^2 g_{0,ss}\theta_s \tag{A.8}$$

where $g_{0,ss}$ is the radial distribution function

$$g_{0,ss}=\left[1-\left(\frac{\alpha_s}{\alpha_{s,max}}\right)^{1/3}\right]^{-1}$$

- Solid bulk viscosity:

$$\lambda_s=\frac{4}{3}\alpha_s\rho_s d_s g_{0,ss}(1+e_{ss})\sqrt{\frac{\theta_s}{\pi}} \tag{A.9}$$

- Solid-phase shear viscosity:

$$\mu_s=\mu_{s,col}+\mu_{s,kin}+\mu_{s,fr} \tag{A.10}$$

$$\mu_{s,col}=\frac{4}{5}\alpha_s\rho_s d_s g_{0,ss}(1+e_{ss})\sqrt{\frac{\theta_s}{\pi}} \tag{A.11}$$

$$\mu_{s,kin}=\frac{\alpha_s d_s\rho_s\sqrt{\theta_s\pi}}{6(3-e_{ss})}\left[1+\frac{2}{5}(1+e_{ss})(3e_{ss}-1)\alpha_s g_{0,ss}\right] \tag{A.12}$$

$$\mu_{s,kin}=\frac{10d_s\rho_s\sqrt{\theta_s\pi}}{96\alpha_s(1+e_{ss})g_{0,ss}}\left[1+\frac{4}{5}g_{0,ss}\alpha_s(1+e_{ss})\right]^2 \tag{A.13}$$

A.4. Shear Stress and Collision Energy at the Wall

$$\tau_s=-\frac{\sqrt{3}\pi\rho_s\alpha_s g_{0,ss}\varphi\sqrt{\theta_s}}{6\alpha_{s,max}}\vec{U}_s \tag{A.14}$$

$$q_s=\frac{\pi}{6}\sqrt{3}\varphi\frac{\alpha_s}{\alpha_{s,max}}\rho_s g_{0,ss}\sqrt{\theta_s}v_{s,w}^2-\frac{\pi}{4}\sqrt{3}\frac{\alpha_s}{\alpha_{s,max}}(1-e_w^2)\rho_s g_{0,ss}\theta_s^{3/2} \tag{A.15}$$